nature COMMUNICATIONS

ARTICLE

Received 22 Jan 2014 | Accepted 15 Jul 2014 | Published 22 Aug 2014

DOI: 10.1038/ncomms5703 OPEN

Nuclear magnetic resonance spectroscopy with single spin sensitivity

C. Müller[1,2,*], X. Kong[1,3,4,*], J.-M. Cai[2,5], K. Melentijević[1,2], A. Stacey[6], M. Markham[6], D. Twitchen[6], J. Isoya[7], S. Pezzagna[8], J. Meijer[8], J.F. Du[3,4], M.B. Plenio[2,5], B. Naydenov[1,2], L.P. McGuinness[1,2] & F. Jelezko[1,2]

Nuclear magnetic resonance spectroscopy and magnetic resonance imaging at the ultimate sensitivity limit of single molecules or single nuclear spins requires fundamentally new detection strategies. The strong coupling regime, when interaction between sensor and sample spins dominates all other interactions, is one such strategy. In this regime, classically forbidden detection of completely unpolarized nuclei is allowed, going beyond statistical fluctuations in magnetization. Here we realize strong coupling between an atomic (nitrogen–vacancy) sensor and sample nuclei to perform nuclear magnetic resonance on four ^{29}Si spins. We exploit the field gradient created by the diamond atomic sensor, in concert with compressed sensing, to realize imaging protocols, enabling individual nuclei to be located with Angstrom precision. The achieved signal-to-noise ratio under ambient conditions allows single nuclear spin sensitivity to be achieved within seconds.

[1] Institute for Quantum Optics, Albert-Einstein Allee 11, University of Ulm, Ulm D-89081, Germany. [2] Center for Integrated Quantum Science and Technology, University of Ulm, Ulm D-89081 Germany. [3] Department of Modern Physics, Hefei National Laboratory for Physics Sciences at Microscale, University of Science and Technology of China, Hefei 230026, China. [4] Synergetic Innovation Center of Quantum Information and Quantum Physics, University of Science and Technology of China, Hefei 230026, China. [5] Institute for Theoretical Physics, Albert-Einstein Allee 11, University of Ulm, Ulm D-89081, Germany. [6] Element Six, Ltd., Ascot, Berkshire SL5 8BP, UK. [7] Research Center for Knowledge Communities, University of Tsukuba, 1-2 Kasuga, Tsukuba, Ibaraki 305-8550, Japan. [8] Experimental Physics II, University Leipzig, Linnéstr. 5, 03401 Leipzig, Germany. * These authors contributed equally to this work. Correspondence and requests for materials should be addressed to L.P.M. (email: liam.mcguinness@uni-ulm.de).

Nuclear magnetic resonance (NMR) spectroscopy is an informative tool routinely used to determine the chemical makeup of macromolecules, including large proteins[1]. Yet the weak interaction strength between sample spins and inductive detectors, and low-thermal polarization, restricts the sensitivity to large ensembles (Fig. 1a). The resolution of imaging techniques is additionally limited by the maximum magnetic gradient that can be applied. By miniaturizing the detector to approach the sample closer, sensor-sample coupling can be increased. Recently, magnetic resonance force microscopy[2,3] and diamond based magnetometers[4–6] have been able to demonstrate NMR on nanoscale ensembles of nuclear spins, improving sensitivity by orders of magnitude compared with the best inductive readout[7]. When noise, in the form of magnetic coupling between sample nuclear spins, exceeds interaction with the sensor, the sensitivity is classically restricted to measurements of statistical fluctuations in sample magnetization[8] (Fig. 1b). However, when coupling between the sensor and measured nuclei dominates over decoherence (strong coupling regime shown in Fig. 1c), individual nuclei may be detected regardless of their polarization. Here we realize such strong coupling by bringing a single electronic spin sensor close to ($\sim$2 nm) weakly interacting ^{29}Si nuclei in a silica layer. Furthermore, strong coupling enables the dipolar field of the atomic sensor to be used as field gradient for magnetic resonance imaging, allowing the positions of four single nuclear spins to be imaged. The ambient experimental methods we demonstrate are an important step towards non-destructive imaging of single biomolecules under physiological conditions, and determining nanoscale structure and composition without ensemble averaging.

The nitrogen–vacancy (NV) defect in diamond is a remarkable magnetic sensor. Optically detected magnetic resonance enables the NV electronic spin to be interrogated by fluorescence microscopy[9], and dipolar interaction with nearby spins—either in the diamond[10–12] or near the surface[13–20] allows spin spectroscopy to be performed. Other applications include nanoscale magnetic field measurements[21,22], bioimaging under ambient conditions[16,23–25] and quantum information processing[26–30]. In the following, we focus on the possibility to achieve direct flip-flops with unpolarized nuclear spins, that is, independent of the initial state of the nuclear spin. The sensitivity of this protocol depends critically on the stand-off distance between the NV sensor and target spins, not only because the interaction strength scales inversely with the third power of the separation distance, but also because the signal characteristics change drastically when the interaction strength between NV and nuclear spins exceeds the coupling between target nuclei. In this strong coupling regime, all nuclear spins directly impart phase accumulation on the NV sensor before spin flips between nuclei occurs, which act to randomize the phase accumulation. The result is a $\sqrt{N}$ enhancement in the signal for detection of N nuclei when compared with the classical case (see Fig. 1b,c), without requiring sample hyperpolarization[31]. The sensitivity we achieve allows in principle a single, unpolarized nuclear spin to be detected within 10 s.

Results

Sensor creation and sensing protocol. A schematic of the experiment is shown in Fig. 2a. NV defects were created by implantation of 2.5 keV N^+ ions into an unpolished diamond surface. Isotopically purified diamond (^{13}C concentration $<$10 p.p.m.) was used to avoid nuclear spin noise from intrinsic ^{13}C nuclei. Shallow NV centres of 2–3 nm depth (Supplementary Table 1) were identified with sub-nanometre precision by placing a standard sample on the surface (see Methods, Supplementary Notes 1–3, Supplementary Figs 1–6). Amorphous silica (SiO_2) was then deposited on the diamond surface. Silica was chosen since it has a low abundance of nuclear spins, ^{29}Si being the most common spin isotope with 4.67% atomic abundance. Use of a dilute spin sample allows the strong coupling regime to be attained, since ^{29}Si nuclear spins at the surface experience a dipolar magnetic field from nearby NV centres, which is stronger than the internuclear coupling, exceeding even the coupling between ^{29}Si dimers (Fig. 2b). In addition, the low density of 1 spin nm^{-3} means on average very few spins are present in the sensing volume (Supplementary Note 4, Supplementary Figs 7 and 8).

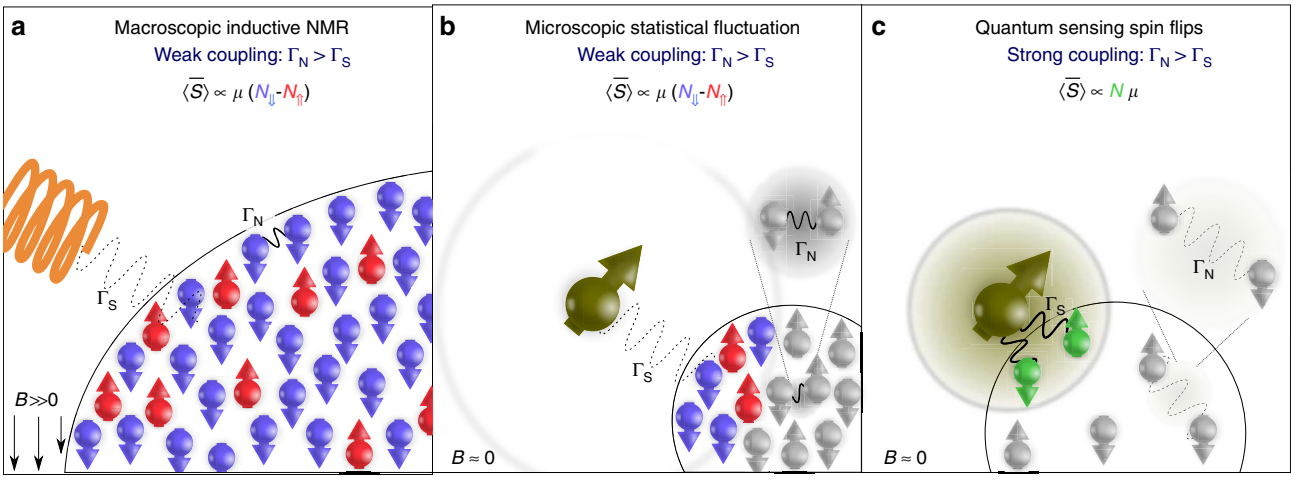

Figure 1 | Classical and quantum NMR detection regimes. (**a**) Inductive NMR: Interaction between the sensor and individual nuclear spins (Γ_S) is much weaker than interaction between nuclei (Γ_N). For large spin ensembles ($\gtrsim 10^{12}$ nuclear spins) the time-averaged signal, $\langle \bar{S} \rangle$ is proportional to the sample polarization (multiplied by the spin magnetic moment, μ). In the high temperature limit, sample magnetization is $\frac{N\mu^2 B}{k_B T}$, where N is the number of spins, B is the external magnetic field, T is the temperature and k_B is the Boltzmann constant. (**b**) Nanoscale NMR: For detection of small ensembles ($\sim 10^4$ nuclear spins) with a weakly coupled sensor, $\langle \bar{S} \rangle$ is still proportional to the sample magnetization. Now statistical fluctuations may exceed thermal polarization, so sample magnetization is given by $\sqrt{N}\mu$. (**c**) Quantum NMR: Detection of individual or few nuclei may occur when interaction of each nuclear spin with the sensor (Γ_S) is stronger than the coupling to the surrounding bath (Γ_N). In this strong coupling regime, the magnetic field of individual spins is measured rather than sample magnetization. The detected signal, $\langle \bar{S} \rangle$, is then proportional to $N\mu$ regardless of whether the nuclei have a net polarization.

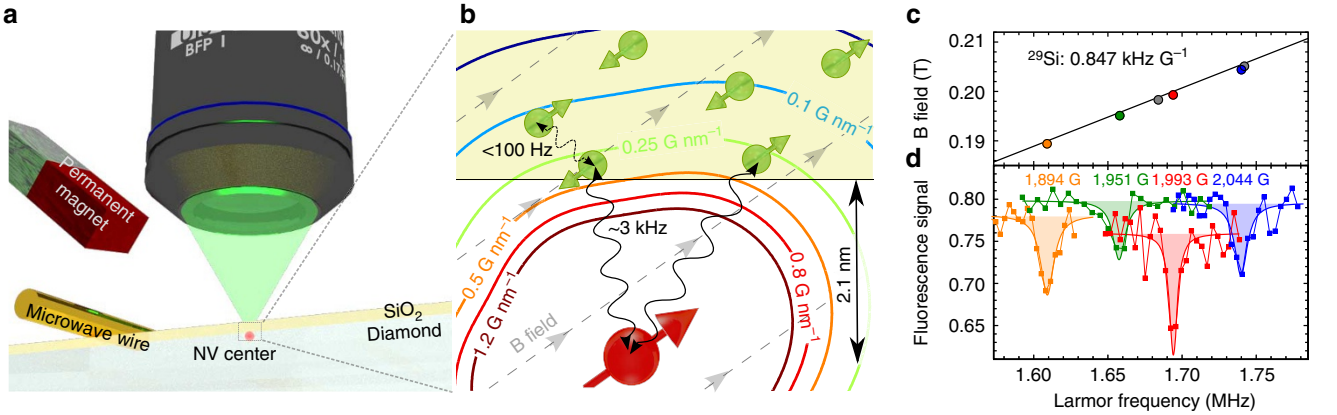

Figure 2 | NMR of ^{29}Si nuclei with a strongly coupled sensor. (**a**) Schematic of the experimental setup. Dilute, unpolarized nuclear spins in a silica layer interact with an electronic spin in a (100)-surface diamond, which is readout with optical microscopy. (**b**) Schematic of strong coupling regime. A shallow NV centre in diamond (2 nm from the surface) couples to nearby ^{29}Si nuclei in a silica layer, due to hyperfine interaction. The contour lines show the strength of the effective magnetic gradient experienced by the nuclear spins. (**c**) Measured ^{29}Si NMR signal as a function of applied magnetic field, using the XY8-*K* decoupling sequence. The detected signal has a slope of 0.847(1) kHz G^{-1} in agreement with the gyromagnetic ratio for ^{29}Si (solid line). The systematic shift of the detected frequency is due to the finite temporal length of decoupling pulses on the NV sensor. (**d**) Measured echo dip for NV centres at different magnetic fields. The signal dependence on the decoupling pulse number can be seen by comparing the data sets at 1,894, 1,951 and 2,044 Gauss (64 pulse acquisition), to the data set at 1,993 Gauss (128 pulse acquisition). Higher-order pulses produce a narrower signal with a stronger dip, up to the decoherence time. Fluorescence contrast has been normalized to the level corresponding to a complete NV spin flip. Measurements at 1,894, 1,993 Gauss were performed on NV-6 with a nominal depth of 2.1 nm, measurements at 1,951, 2,044 Gauss were performed on NV-7 with a depth of 2.3 nm.

To detect hyperfine interaction between the NV defect and N unpolarized nuclei, we bring the NV spin into resonance with nuclear spins, and then read the phase acquired by the NV due to interaction with the nuclei. Nuclear evolution is governed by the Hamiltonian:

$$H = \omega_L \sum_n^N \mathbf{I}_n^Z + \mathbf{S}_Z \sum_n^N \left(\alpha_n \mathbf{I}_n^Z + \beta_n \cdot \mathbf{I}_n^\perp\right), \qquad (1)$$

where $\mathbf{S}_i$ and $\mathbf{I}_i$ are the NV electron and ^{29}Si nuclear spin operators respectively, ω_L is the Larmor frequency, and α, β are the parallel and perpendicular components of the hyperfine coupling (see Supplementary Note 5). The hyperfine interaction (second term of Eq. 1) is zero for NV in the $|m_s=0\rangle$ state of the magnetic ground-state triplet, whereas for the NV $|m_s=-1\rangle$ state, each nuclear spin rotates about an axis set by the vector sum of the external magnetic field and the positional-dependent hyperfine field. By repeated adjustments of the NV spin state in synchrony with nuclear evolution, the nuclear trajectory can be tailored to allow a complete flip, (in concert with an NV flop)—in effect, amplifying the conditional interaction. The rate of this rotation is given by the perpendicular component (β) of the hyperfine interaction, and we emphasize that rotation occurs independently of whether the nucleus was initially spin up or spin down. For several nuclei each with individual coupling rates, the dynamics of the sensor become complex; however, in the short time limit investigated here, the overall signal closely approximates a linear sum of individual contributions (see Supplementary Note 6 and Supplementary Figs 9–12). The particular pulse sequence we used to adjust the NV spin state in time with nuclear evolution was the XY8-*K* pulse sequence, as it is robust against pulse errors[32]. The optimum timing of pulses on the NV spin to produce a spin flip is given by

$$\tau = (2m-1)/2f_n = (2m-1)\pi/(\omega_L + \alpha_n), \qquad (2)$$

where $m = 1, 3, 5 \ldots$, arises due to the periodicity of the rotation—referred to as the order of the dip[10], and f_n is the frequency of each nuclear spin, which may be shifted from the bare Larmor frequency by hyperfine interaction with the NV spin. Dynamical decoupling also protects the NV from unwanted spin noise, in particular at high fields where the decoupling pulses are dense, and for this reason, we operated at magnetic fields of $\sim$0.2 T.

NMR spectroscopy of few nuclear spins. In Fig. 2c,d, we plot the measured XY8 spin echo for NV spins below the silica interface, which shows a clear dip near the ^{29}Si Larmor frequency, due to the relative phase acquired by the NV. Analysis of the signal strength gives agreement for interaction with six to eight nuclear spins, where we have taken into account the depth of the NV centres and the expected ^{29}Si density. We have verified with the parameters in our experiments ($\omega_L \gg \alpha_n, \beta_n$), that the dependence of the signal on the ^{29}Si nuclear spin polarization is negligible, thus demonstrating a new detection regime of NMR (more details are available in Supplementary Notes 4,5 and Supplementary Fig. 9). We are also able to estimate the coupling strength between NV and nuclei from the signal contrast over the measurement time. The 8% contrast we obtain over the interaction time (19 μs) gives an average coupling strength to individual nuclei on the order of 3 kHz, consistent with the perpendicular component of the hyperfine interaction for a separation between NV electron spin and ^{29}Si nuclear spins of 2 nm.

Magnetic resonance imaging of individual nuclear spins. To resolve the hyperfine couplings of individual ^{29}Si nuclei, we increased the number of decoupling pulses, thereby improving the spectral resolution. For a classical spin bath where a large number of equivalent spins interact weakly with the NV centre[4,5], the echo dip is centred at the nuclear Larmor frequency, and its width, $\Delta\omega$ scales with the sensitivity function of the echo, $\Delta\omega/2\pi \approx 1/K\tau$, where K is the total number of pulses. However, in the case of strong interaction between nuclei and electron spin sensor, individual nuclei become detuned and the width of the echo dip is given by the inhomogeneous broadening resulting from the field gradient created by the electron spin[10–12]. Here we use the 0.05 mT nm^{-1} magnetic gradient at separations of 2 nm between the atomic scale NV sensor and silicon spins, as a unique opportunity for nanoscale imaging.

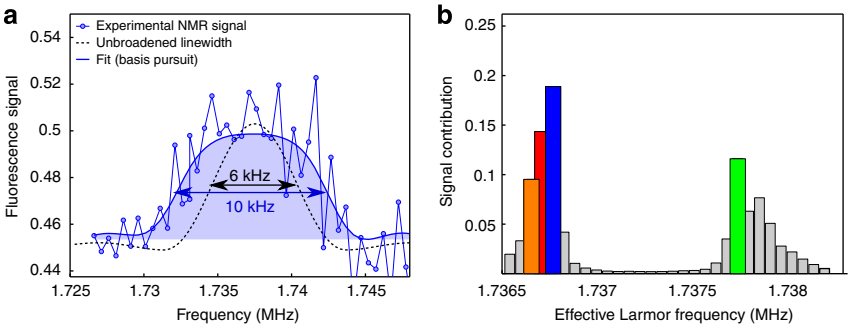

Figure 3 | NV gradient separation of individual ^{29}Si nuclei. (**a**) Under high-order decoupling (XY8-512 pulse sequence), inhomogeneous broadening of the ^{29}Si NMR line due to the NV magnetic gradient can be observed. The expected line width of the XY8-512 sequence for weakly interacting nuclear spins is shown as the black dotted line with a FWHM of 6 kHz. The blue solid line is the best fit to the data using basis pursuit (see Supplementary Note 7 for technical details) showing an additional broadening of 4 kHz. (**b**) Using BPDN, we calculate the Larmor frequency and relative contribution of 50 nuclear spins comprising the total signal (see Methods). These are plotted individually, with the four strongest highlighted, which contribute to more than 50% of the signal.

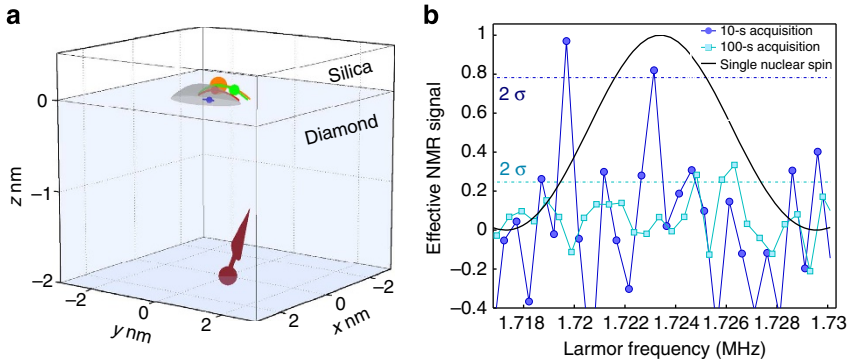

Figure 4 | Imaging of nuclear positions and single spin sensitivity. (**a**) The best fit locations of the four strongest contributing ^{29}Si nuclei as obtained from basis pursuit are shown as the coloured arcs (colour corresponds with Fig. 3b). A representative position of each spin is denoted with a filled ball, and the positional uncertainty in the *x* and *z* directions is given by the size of the ball. Maximal uncertainties from BPDN are $\Delta x = \pm 0.2$ nm, $\Delta z = \pm 0.1$ nm. The circular symmetry of the field pattern greatly increases the uncertainty around the azimuthal angle, here it is limited by intersection with the diamond surface; as a result, the resolution in *y* is 0.1 nm for the nearest spin and increases to 0.5 nm for the furthest spin (see Supplementary Note 9). The surface of the hyperfine pattern with a strength equal to the signal plotted in (**b**) is shown in grey. (**b**) Expected NMR signal for the case of a single ^{29}Si nuclear spin on the surface of the 0.5 nm^3 volume shown in (**a**). The signal exceeds the shot noise limit by more than two s.d. values for a 9.7 s acquisition per time point (dark circles).

Under higher-order decoupling, inhomogeneous broadening of the NMR signal becomes apparent (Fig. 3a), but broad-band magnetic noise prevented observation of full electron-nuclear flip-flops and thus fully resolved lines. We were nevertheless able to gain deeper insight into the location and detuning of individual nuclear spins by employing advanced methods from signal processing. Indeed, the frequencies of individual nuclei while not being immediately resolvable can be extracted using the superresolution properties of basis pursuit de-noising[33] (BPDN, see Methods, Supplementary Notes 7 and 8, Supplementary Figs 13–16). Figure 3b shows the obtained spectral decomposition of the contributing nuclear spins and their hyperfine coupling parameters, suggesting that four nuclei account for more than 50% of the signal (Supplementary Fig. 15), which is of comparable size to many chemical functional groups and below the size of a small amino acid.

To demonstrate how structural information and imaging may be obtained, we plot the best fit locations of silicon nuclei as recovered from BPDN (Fig. 4a). The two-component (α, β) anisotropy of the hyperfine interaction allows assignment of a unique location for each nuclear spin up to one degree of circular symmetry, with respect to the NV axis. Despite the extra degree of freedom, we are still able to estimate the location of two nuclei with an uncertainty below 0.2 nanometres (Supplementary Note 9, Supplementary Fig. 17). Techniques which break the circular symmetry (Supplementary Note 10) and longer data acquisition times can be used to reduce the spatial resolution below one Angstrom.

Single nuclear spin sensitivity. The signal-to-noise ratio of the experiments presented here reaches the ultimate sensitivity limit of NMR spectroscopy (Fig. 4b). We show that for a single point measurement time of 10 s, the signal from a single nuclear spin exceeds shot noise by more than two s.d. values. With a sensing volume on the order of a cubic nanometre and single spin sensitivity, the direct discrimination of single molecules based on differences of one atom at a functional site appears feasible. As further confirmation of detection in the strong coupling regime, we note the scaling of the signal with distance from diamond surface *r* is also stronger than the classical case, closely following r^{-3} behaviour (Supplementary Note 6).

Discussion

The results presented in this paper show that by operating in the strong coupling regime, the sensitivity of NMR and imaging can

be extended to single nuclear spins. The technique can be applied to perform two-dimensional NMR[34] on single biomolecules with spatial resolution well below the size of a protein and thus allow for label-free detection. Further improvements in decoupling techniques will allow a spectral resolution limited by the electron spin relaxation time[35] ($\sim$100 Hz for NVs measured here). Although the strong coupling regime reported in this paper allows for polarization-independent NMR, the possibility to transfer NV polarization to nearby nuclei[36–38] will allow for investigations of internuclear couplings and nuclear Overhauser effect. Nuclear decoupling techniques will also allow strong coupling to be achieved in dense spin samples, providing a signal independent of nuclear polarization[39,40].

In addition, as demonstrated here, benefits can be derived from the use of signal processing methods to extract more detailed information about spins contributing to the signal and can also allow for a significant reduction in the number of data points required[41]. Direct manipulation of nuclear spins using radiofrequency fields may be utilized as a high resolution spectroscopy tool for detection of chemical shifts, giving information on the three dimensional structure of molecules[5,42]. Alternatively, electron spin labels providing pseudocontact chemical shifts[43] may be employed to enable direct resolution of individual nuclei in single molecules.

Methods

Calibration of NV depth and sensing volume. To identify shallow NV centres, we measured the nuclear magnetic signal at the Larmor frequency of ^{1}H using the XY8-K dynamical decoupling sequence. Initial characterization was performed with a dense nuclear spin sample—immersion oil (Fluka Analytical 10976). The signal remained in the weak coupling regime; therefore, we use a classical treatment[4]. First, we measure the magnetic field fluctuation $\langle \Delta B^2 \rangle$, from protons in the oil by integrating the power spectral density $S(\omega)$, see Supplementary Fig. 4:

$$\langle \Delta B^2 \rangle = \frac{1}{2\pi} \int_{-\infty}^{\infty} S(\omega) d\omega. \qquad (3)$$

For NV-6, plotted in Fig. 2, we obtain $\sqrt{\langle \Delta B^2 \rangle} \approx 0.072$ MHz (2.58 μT), further details can be found in Supplementary Note 3. If we assume the protons to be homogeneously distributed with a density ρ on the diamond surface in a layer of thickness h, we obtain the magnetic field sensed by an NV centre in a depth r below the diamond surface by[19]:

$$\sqrt{\langle \Delta B^2 \rangle} = \mu_H \mu_0 \sqrt{\frac{5\rho}{384\pi}} \sqrt{\frac{1}{r^3} - \frac{1}{(r+h)^3}} \qquad (4)$$

where $\mu_H = 1.41 \times 10^{-26} J \cdot T^{-1}$ is the nuclear magneton of hydrogen and μ_0 the vacuum permeability. For a proton density of 50 nm^{-3}, and a sample thickness exceeding 10 nm, the measured magnetic field leads to a depth estimate of 2.1 nm, with an error dominated by uncertainty in the oil density (Supplementary Fig. 5). To determine the sensing volume, we analysed the signal as a function of number of nuclear spins, showing that 390–400 nuclei make the most significant contribution to the signal, corresponding to a volume of 8 nm^3 above the diamond surface (more details in Supplementary Note 3 and Supplementary Fig. 6).

Deposition of amorphous silica on diamond surface. After identification of shallow NV centres, diamonds were cleaned in a 1:1:1 admixture of three acids (H_2SO_4:$HClO_4$:HNO_3) at 180 °C for several hours. After cleaning, the diamonds were transferred to chromatography grade water before $\sim$10 μl of a 1:1 solution of (tetraethyl orthosilicate:ethanol) was dropped onto the surface. We also observed comparable results when depositing undiluted tetraethyl orthosilicate onto a diamond surface directly taken from water. Diamond substrates were then placed onto a hotplate at 120 °C for 10 min.

Basis pursuit analysis. BPDN determines signal representations from overcomplete dictionaries of signal forms by convex optimization[33]. The total signal, $\chi(\tau)$ we observe, arises from ^{29}Si nuclei and background noise (Supplementary Fig. 10), namely $\chi(\tau) = \chi_{Si}(\tau) + \chi_{bg}(\tau)$, with the total contribution from ^{29}Si nuclei, $\chi_{Si}(\tau)$ being summed over all N individual nuclei, $\chi_{Si}(\tau) = \sum_n^N \chi_{Si}^{(n)}$. To perform this analysis, we assume that the contribution of individual ^{29}Si takes the form of a normalized filter function:

$$\chi_{Si}^{(n)}(\tau) = \frac{4}{K^2} \sin^4\left(\frac{\omega_n \tau}{4}\right) \sin^2\left(\frac{\omega_n K \tau}{2}\right) / \cos^2\left(\frac{\omega_n \tau}{2}\right), \qquad (5)$$

which is based on the assumption that each individual ^{29}Si generates a magnetic field with a delta (effective Larmor) frequency ω_n. An exact numerical simulation using the full Hamiltonian suggests that the shape of the above basis function agrees very well with the shape of the echo decay caused by a single ^{29}Si with a typical distance of 2–3 nm to the NV centre. The experimental data provide us with a series of function values for the echo decay $C_{exp}(\tau)$. The task that BPDN solves is to reproduce the observed signal to a desired precision using a superposition of the smallest number of dictionary elements (that is, ^{29}Si nuclear spins). That is we solve the optimization problem

$$\min_{b_M \geq b \geq 0} \frac{1}{2} \left\| \frac{1}{2} \left[1 + e^{-\sum_{j=1}^{J} b_j \chi_{Si}^{(j)}} e^{-\chi_{bg}(\tau)} \right] - C_{exp}(\tau) \right\|_2^2 + \lambda \sum_{j=1}^{J} |b_j|, \qquad (6)$$

where $b_{j \geq 0}$ quantifies the contribution of each basis function to the total signal and can be identified with perpendicular component of the hyperfine coupling by a scaling factor, b_M is the maximum value b_j may take, given an NV depth of 2 nm. The value of λ determines how well the fitting data should agree with the experiment data, and J is the number of basis functions. We chose $J = 30$, meaning we take into account 30 spins to describe the signal. From the silica density, this gives a contributing volume of $\sim$25–30 nm^3 much greater than the sensing volume, and beyond this distance, the strong coupling regime no longer holds. Using BPDN, we are able to reproduce the experimental data with very good agreement. For a smaller value of λ, the solution becomes close to the exact basis pursuit, and the fitting shows better agreement with the experiment (see Supplementary Fig. 14 and details in Supplementary Note 7).

The estimation of the number of ^{29}Si that produce the observed signal is robust when varying the parameter λ in BPDN as long as the fitting is above a certain confidence level, see Supplementary Note 7. We have verified the validity of the optimal values of b_n and ω_n obtained: the amplitudes b_n are consistent with a distance to the NV centre of around 2 nm and the distribution of ω_n that make largest contribution are within a few kHz.

References

1. Wüthrich, K. Protein structure determination in solution by NMR spectroscopy. *J. Biol. Chem.* **265,** 22059–22062 (1990).
2. Mamin, H. J., Poggio, M., Degen, C. L. & Rugar, D. Nuclear magnetic resonance imaging with 90-nm resolution. *Nat. Nanotechnol.* **2,** 301–306 (2007).
3. Degen, C. L., Poggio, M., Mamin, H. J., Rettner, C. T. & Rugar, D. Nanoscale magnetic resonance imaging. *Proc. Natl Acad. Sci.* **106,** 1313–1317 (2009).
4. Staudacher, T. *et al.* Nuclear magnetic resonance spectroscopy on a (5-Nanometer)^3 sample volume. *Science* **339,** 561–563 (2013).
5. Mamin, H. J. *et al.* Nanoscale nuclear magnetic resonance with a nitrogen-vacancy spin sensor. *Science* **339,** 557–560 (2013).
6. Ohashi, K. *et al.* Negatively charged nitrogen-vacancy centers in a 5 nm thin ^{12}C diamond film. *Nano Lett.* **13,** 4733–4738 (2013).
7. Sakellariou, D., Le Goff, G. & Jaquinot., J.-F. High-resolution, high-sensitivity NMR of nanolitre anisotropic samples by coil spinning. *Nature* **447,** 694–697 (2007).
8. Bloch, F. Nuclear induction. *Phys. Rev.* **70,** 460–474 (1946).
9. Jelezko, F. & Wrachtrup, J. Read-out of single spins by optical spectroscopy. *J. Phys. Condens. Matter* **16,** R1089–R1104 (2004).
10. Taminiau, T. H. *et al.* Detection and control of individual nuclear spins using a weakly coupled electron spin. *Phys. Rev. Lett.* **109,** 137602 (2012).
11. Kolkowitz, S., Unterreithmeier, Q. P., Bennett, S. D. & Lukin, M. D. Sensing distant nuclear spins with a single electron spin. *Phys. Rev. Lett.* **109,** 137601 (2012).
12. Zhao, N. *et al.* Sensing single remote nuclear spins. *Nat. Nanotechnol.* **7,** 657–662 (2012).
13. Grotz, B. *et al.* Sensing external spins with nitrogen-vacancy diamond. *New J. Phys.* **13,** 055004 (2011).
14. Mamin, H. J., Sherwood, M. H. & Rugar, D. Detecting external electron spins using nitrogen-vacancy centers. *Phys. Rev. B* **86,** 195422 (2012).
15. McGuinness, L. P. *et al.* Ambient nanoscale sensing with single spins using quantum decoherence. *New J. Phys.* **15,** 073042 (2013).
16. Steinert, S. *et al.* Magnetic spin imaging under ambient conditions with sub-cellular resolution. *Nat. Commun.* **4,** 1607 (2012).
17. Ermakova, A. *et al.* Detection of few metallo-protein molecules using color centers in nanodiamonds. *Nano Lett.* **13,** 3305–3309 (2013).
18. Ziem, F. C., Götz, N. S., Zappe, A., Steinert, S. & Wrachtrup, J. Highly sensitive detection of physiological spins in a microfluidic device. *Nano Lett.* **13,** 4093–4098 (2013).

19. Loretz, M., Pezzagna, S., Meijer, J. & Degen, C. L. Nanoscale nuclear magnetic resonance with a 1.9-nm-deep nitrogen-vacancy sensor. *Appl. Phys. Lett.* **104,** 033102 (2014).
20. Grinolds, M. S. *et al.* Subnanometer resolution in three-dimensional magnetic resonance imaging of individual dark spins. *Nat. Nanotechnol.* **9,** 279–284 (2014).
21. Balasubramanian, G. *et al.* Nanoscale imaging magnetometry with diamond spins under ambient conditions. *Nature* **455,** 648–651 (2008).
22. Maze, J. R. *et al.* Nanoscale magnetic sensing with an individual electronic spin in diamond. *Nature* **455,** 644–647 (2008).
23. Le Sage, D. *et al.* Optical magnetic imaging of living cells. *Nature* **496,** 486–489 (2013).
24. McGuinness, L. P. *et al.* Quantum measurement and orientation tracking of fluorescent nanodiamonds inside living cells. *Nat. Nanotechnol.* **6,** 358–363 (2011).
25. Kucsko, G. *et al.* Nanometre-scale thermometry in a living cell. *Nature* **500,** 54–58 (2013).
26. Neumann, P. *et al.* Multipartite entanglement among single spins in diamond. *Science* **320,** 1326–1329 (2008).
27. Neumann, P. *et al.* Single-shot readout of a single nuclear spin. *Science* **329,** 542–544 (2010).
28. Dutt, M. V. G. *et al.* Quantum register based on individual electronic and nuclear spin qubits in diamond. *Science* **316,** 1312–1316 (2007).
29. Buckley, B. B., Fuchs, G. D., Bassett, L. C. & Awschalom., D. D. Spin-light coherence for single-spin measurement and control in diamond. *Science* **330,** 1212–1215 (2010).
30. Robledo, L. *et al.* High-fidelity projective read-out of a solid-state spin quantum register. *Nature* **477,** 574–578 (2011).
31. Ardenkjaer-Larsen, J. H. *et al.* Increase in signal-to-noise ratio of $>$ 10,000 times in liquid-state NMR. *Proc. Natl. Acad. Sci.* **100,** 10158–10163 (2003).
32. Gullion, T., Baker, D. B. & Conradi, M. S. New, compensated Carr-Purcell sequences. *J. Magn. Reson.* **89,** 479–484 (1990).
33. Chen, S. S., Donoho, D. L. & Saunders, M. A. Atomic decomposition by basis pursuit. *SIAM Rev.* **43,** 129–159 (2001).
34. Amero, C. *et al.* Fast two-dimensional NMR spectroscopy of high molecular weight protein assemblies. *J. Am. Chem. Soc.* **131,** 3448–3449 (2009).
35. Laraoui, A. *et al.* High-resolution correlation spectroscopy of ^{13}C spins near a nitrogen-vacancy centre in diamond. *Nat. Commun.* **4,** 1651 (2013).
36. Jacques, V. *et al.* Dynamic polarization of single nuclear spins by optical pumping of nitrogen-vacancy color centers in diamond at room temperature. *Phys. Rev. Lett.* **102,** 4 (2009).
37. Wang, H.-J. *et al.* Sensitive magnetic control of ensemble nuclear spin hyperpolarization in diamond. *Nat. Commun.* **4,** 1940 (2013).
38. London, P. *et al.* Detecting and polarizing nuclear spins with double resonance on a single electron spin. *Phys. Rev. Lett.* **111,** 067601 (2013).
39. Lee, M. & Goldburg., W. I. Nuclear-magnetic-resonance line narrowing by a rotating rf field. *Phys. Rev.* **140,** A1261–A1271 (1965).
40. Cai, J., Jelezko, F., Plenio, M. B. & Retzker., A. Diamond-based single-molecule magnetic resonance spectroscopy. *New J. Phys.* **15,** 013020 (2013).
41. Almeida, J., Prior, J. & Plenio, M. B. Computation of two-dimensional spectra assisted by compressed sampling. *J. Phys. Chem. Lett.* **3,** 2692–2696 (2012).
42. Perunicic, V. S., Hall, L. T., Simpson, D. A., Hill, C. D. & Hollenberg., L. C. L. Towards single-molecule NMR detection and spectroscopy using single spins in diamond. *Phys. Rev. B* **89,** 054432 (2013).
43. Mayo, B. Lanthanide shift reagents in nuclear magnetic resonance spectroscopy. *Chem. Soc. Rev.* **2,** 49–74 (1973).

Acknowledgements

We thank Michael Ferner and Manfred Bürzele for technical assistance with experiments, Holger Gerster and Chemische Fabrik Karl Bucher for suggesting tetraethyl orthosilicate and Friedemann Reinhard and Robert Scholten for useful discussions. We acknowledge DARPA, JST, EU (ERC Synergy grant BioQ, DIAMANT, SIQS), DFG (SFB TR 21, FOR 1493, FOR 1482), the 973 Program (2013CB921800), NNSFC (11227901, 91021005), Alexander von Humboldt and Volkswagen foundations for funding.

Author contributions

C.M., X.K., K.M., L.P.M. and F.J. performed the experiments. J.-M.C. and M.B.P analysed the data and performed basis pursuit de-noising. A.S., M.M., D.T. and J.I. provided diamond substrates. S.P. and J.M. performed the implantation. J.F. D., J.-M.C., M.B.P., B.N., L.P.M. and F.J. planned and coordinated the project. J.-M.C., M.B.P., L.P.M. and F.J. wrote the manuscript with contributions from all authors.

Additional information

Supplementary Information accompanies this paper at http://www.nature.com/naturecommunications

Competing financial interests: The authors declare no competing financial interests.

Reprints and permission information is available online at http://npg.nature.com/reprintsandpermissions/

How to cite this article: Müller, C. *et al.* Nuclear magnetic resonance spectroscopy with single spin sensitivity. *Nat. Commun.* 5:4703 doi: 10.1038/ncomms5703 (2014).